Innovation and discovery of graphene-like materials via density-functional theory computations

Qing Tang,[1] Zhen Zhou[1]* and Zhongfang Chen[2]*

Inspired by the intensive studies of graphene, scientists have put extraordinary efforts in exploring properties and phenomena involving noncarbon graphene-like two-dimensional (2D) nanomaterials, particularly those only consisting of single layers or few layers. Experimentally, many graphene-like 2D structures have been fabricated from a large variety of layered and nonlayered materials. These graphene-like structures have already shown exceptional properties, which will offer new breakthroughs and innovative opportunities in nanomaterials science. Theoretically, density-functional theory (DFT) computations offer a powerful tool to investigate the electronic structure (principally the ground state) of nanomaterials, to predict their intrinsic properties, assist in characterization, and rationalization of experimental findings, as well as explore their potential applications. By DFT computations, many graphene-like materials have been explored and designed, and fantastic properties are disclosed. In this review, we present the recent computational progress in discovering the intrinsic structural, electronic, and magnetic properties of several important and representative graphene-like 2D nanomaterials, as well as identifying their potential applications. The highlighted graphene-like structures include layered van der Waals (vdW) materials (h-BN, MoS_2, α-MoO_3, and V_2O_5), graphitic-like ZnO, MXenes (metal carbides or carbonitrides), the not-yet-synthesized B_2C, SiC_2, BSi_3, arsenene and antimonene, and single-layer coordination polymers ($[Cu_2Br(IN)_2]_n$ (IN = isonicotinato), Fe-phthalocyanine, and nickel bis(dithiolene)). © 2015 John Wiley & Sons, Ltd

*Correspondence to: zhouzhen@nankai.edu.cn; zhongfangchen@gmail.com

[1]Key Laboratory of Advanced Energy Materials Chemistry (Ministry of Education), Computational Centre for Molecular Science, Institute of New Energy Material Chemistry, Collaborative Innovation Center of Chemical Science and Engineering (Tianjin), School of Materials Science and Engineering, National Institute of Advanced Materials, Nankai University, Tianjin, PR China

[2]Department of Chemistry, Institute for Functional Nanomaterials, University of Puerto Rico, San Juan, PR, USA

Conflict of interest: The authors have declared no conflicts of interest for this article.

INTRODUCTION

The discovery of graphene has fueled fundamental interest in two-dimensional (2D) nanomaterials.[1] Graphene is attractive because it possesses extraordinary properties and demonstrates strong potential for future electronics. Though overwhelmed, graphene is not the single child in the family of 2D nanomaterials. Other graphene-like nanomaterials, such as hexagonal BN (*h*-BN), metal dichalcogenides, oxides, and carbides, also joined the 2D family.[2–8] It was the tremendous efforts of the peers in synthesizing these graphene-like 2D materials that made it possible to investigate their intrinsic properties and explore their potential applications. Many such 2D nanomaterials have been

experimentally achieved, such as single- or few-layer *h*-BN, MoS_2, MXene, and coordination polymers (CPs).

By means of density-functional theory (DFT) computations, researchers have explored many graphene-like materials. For example, the electronic properties of BN and MoS_2 nanoribbons depend heavily on edge shapes, and can be modified by defects, doping, and surface or edge functionalizations[9–11]; polar (0001) untrathin films of Wurtzite ZnO would transform into graphitic-like structures[12]; planar tetracoordinate carbon- and silicon-containing B_2C[13] and SiC_2[14] were designed. Excitingly, several predications, for example, depolarized ZnO(0001) monolayer[15] and MoS_2 nanoribbon[16] were confirmed experimentally rather shortly.

The main goal of this review is to discuss recent DFT computational efforts in understanding the intrinsic structural, electronic, and magnetic properties, establishing structure-property relationship, and identifying promising applications of several important and representative graphene-like materials.

THEORETICAL FRAMEWORKS: STRENGTHS AND LIMITATIONS OF DFT

As the most widely used quantum mechanics or 'ab-initio' method, DFT serves as the basis for much of the condensed-matter physics and quantum chemistry, and offers a powerful tool for computing electronic and other properties of a large number of materials ranging from the bulk phase to low-dimensional nanostructures.

DFT is based on the Hohenberg–Kohn theorem that the properties of a system are a function of the electron density, and is implemented by solving the Kohn–Sham equations, which maps the intractable many-body system of interacting electrons into a fictitious but simplified system of noninteracting electrons moving in an effective potential. The exchange and correlation (XC) effects contain all the complications due to the quantum nature of the electrons, and are accounted by the XC potential, which is approximated by functionals, such as the local density approximation (LDA), the generalized gradient approximation (GGA), and hybrid functionals. Generally, DFT can yield a qualitatively, sometimes even quantitatively, correct picture of the ground-state geometries, vibrational properties, and electronic structures of molecules, crystals, and surface systems.

Within the frameworks of DFT, we have lots of choices on the basis sets and exchange correlation functional, and different computing codes are available.

Taking both the computational efficiency and the computational accuracy into account, for 2D materials, the mostly used basis sets are plane-wave basis set (VASP or CASTEP software code),[17] projector-augmented-wave (PAW) pseudopotential or ultrasoft (US) pseudopotential, and the numerical atomic-orbital basis set plus p-polarization functions (DNP) or d-polarization functions (DND) including all-electron semi-local or effective core pseudopotentials ($DMol^3$ code).[18] The functionals of choice include GGA functionals of Perdew-Wang (PW91) or (Revised) Perdew-Burke-Eruzerhof [(R)PBE],[19] LDA functionals of Ceperley Alder (CA) or Troullier–Martins (TM).[20] Typically, all the supercell structures are treated with periodic boundary conditions (PBCs). Particularly, the GGA/PBE can give the lattice parameters of crystals very close to the experiment, which pushes the accuracy within the 1% range.

When addressing the dynamic effects of extended materials, the first-principles-based approach, such as *ab-initio* molecular dynamics (AIMDs), where the forces are calculated from accurate electronic structure calculations, is very attractive.

Although DFT has become an important working tool in studying a variety of electronic and structural properties of nanomaterials, the standard DFT method has its inherent limitations, and it remains a major challenge in the theoretical community to improve its accuracy and efficiency. In the following discussion, we will shortly document a few challenges when dealing with the structure and electronic properties of 2D nanomaterials.

The first challenge is to get accurate band gaps. A proper reproduction of the experimental band gap in semiconducting or insulating materials is a necessary prerequisite in order to accurately describe the electronic structure and/or optical properties. Currently, the most accurate method for band-gap computations is GW approach of many-body perturbation theory, which is too expensive for 2D materials. The most commonly used local and semilocal approximations to the exchange-correlation functional in standard DFT tend to severely underestimate the band gaps of semiconductors, thus the computed band gaps can only be used for qualitative comparison with experimental data. Fortunately, the trend of the band-gap changes predicted by DFT is typically correct. As far as the 'band-gap problem' is concerned, the recently developed screened exchange hybrid density functional, namely HSE06,[21] provides a good solution in many cases. HSE06 is designed to reproduce exchange energies comparable to traditional hybrids while only using the short range, screened HF exchange (usually with a mixing parameter of 0.25, but can be individually adapted for each

investigated system), thus, it is often used as a compromise between accuracy and computational efficiency (the computational time required for HSE calculations is about a factor of 2–4 higher than pure DFT, while the band-gap calculation using HSE produces error over five times smaller than pure DFT). However, note that the Heyd-Scuseria-Ernzerhof (HSE) should be only considered as an improvement in band-gap accuracy compared with LDA and GGA, but not a method to fully rely on.[22]

The second challenge is to well describe dispersion interactions in 2D materials. Note that the reliable determination on the geometry and cohesive (binding) energies of layered van der Waals (vdW) solids or the physical adsorption of molecules on the inorganic substrates is essential to understand and design such materials. By nature, the dispersion energies are related to interactions between electrons separated by distances of several angstroms; however, standard DFT models commonly use semilocal correlation functionals, counted only for separations of the order of 1 Å distance, but neglect nonlocal long-range dispersion interactions. In other words, standard DFT methods can provide an accurate description of strong covalent and ionic bonds, but fail badly for systems with substantial nonlocal dispersion interactions. One solution to well describe noncovalent systems is to supplement the standard Kohn–Sham-DFT energies with semiempirical dispersion corrections (the damped C_6R^{-6} term as an add-on correction), leading to the so-called DFT +D approaches (DFT-D1, DFT-D2).[23,24] Particularly, the recently implemented DFT-D3 method has been fined with higher accuracy, where the dispersion coefficients (C_6) and atom pairwise cutoff radii (R) are less empirical and both are computed from first principles.[25]

The third challenge is to handle the intrinsic self-interaction error, especially in strongly correlated systems. The inexact exchange energy approximation in DFT introduces self-interaction errors (SIEs), and consequently results in overly delocalized electron densities. SIEs become very significant in strongly correlated transition-metal-oxide systems with robustly localized d or f electrons, and their electronic (such as band gaps and defect energy levels) and magnetic (magnetic ground states) behaviors can be improperly predicted by standard DFT. A commonly used SIE correcting approach to improve the description of d and f electrons in transition metal oxides is the DFT+U method.[26] The basic idea behind DFT+U theory is to treat the strong on-site Coulomb interaction of localized electrons with an additional Hubbard-like term (applying an averaged intra-atomic interaction potential between the strongly correlated

electrons). The strengths of the on-site interactions are usually described by parameters U (on site Coulomb) and J (on site exchange). The computationally effective treatment of DFT+U depends only on the difference, $U_{eff} = U–J$. The parameters U and J can, in principle, be extracted from *ab-initio* calculations. In reality, however, both U and J values are usually determined semi-empirically, by fitting specific physical property to experimental data, such as the crystal lattice parameters and band gap.

GRAPHENE-LIKE MATERIALS ACHIEVED FROM LAYERED MATERIALS WITH vdW INTERLAYER INTERACTION

In this section, we restrict our discussion to graphite-like layered structures with strong in-plane covalent bonds while the adjacent sheets are stacked by weak vdW forces, and the typical examples are *h*-BN, MoS_2, and oxides (α-MoO_3 and V_2O_5).

Because of the weak interlayer interactions, these layered solids can be easily exfoliated into single or few layers. The recent experimental achievements in synthesizing these 2D nanostructures are quite encouraging.[3,27,28]

Along with experimental achievements, computational investigations on these vdW structures also progressed with great pace, leading to discoveries of interesting properties. Based on their structural characteristics, these materials are categorized into planar (*h*-BN) and nonplanar ones (MoS_2, α-MoO_3, and V_2O_5). Among them, the simplest form is the atomically thin BN sheets, while the nanosheets of MoS_2, α-MoO_3, and V_2O_5 all have complicated anisotropic bonding. On the other hand, both BN and MoS_2 have hexagonal symmetry similar to graphite, whereas α-MoO_3 and V_2O_5 have orthorhombic symmetry.

Planar (*h*-BN)

Layered *h*-BN is isostructural to graphite, and its monolayer is the nearest heteroatomic analogue of graphene. Despite their structural similarity, the electronic properties differ dramatically: graphene is a zero-band-gap semimetal, while *h*-BN monolayer is a wide-band-gap semiconductor (band gap: ~6 eV).[29] Owing to its electrical insulating property, *h*-BN has been applied to ultraviolet-light laser devices,[30] field emitters,[31] and nanofillers in polymer composites.[32] Particularly, because of good lattice match and atomically smooth surface free of dangling bonds, *h*-BN

nanosheets serve as excellent dielectric layers for graphene-based electronics.[33,34]

Compared with the medium band gap desired for most semiconductor industries, the wide-band gap constitutes a severe obstacle for applying *h*-BN to electronic and optoelectronic devices. It is thus of great demand to search for ways to control the electronic properties of *h*-BN. Several methods have been proposed in theory, such as cutting into nanoribbons, introducing structural defects, doping, and modifying edge or surface chemically.

Motivated by the fascinating properties of graphene nanoribbons, there is also great interest in BN nanoribbons (BNNRs), which have been experimentally produced by unzipping of BN nanotubes.[3,35–37] Armchair BNNRs are robust semiconductors, whether the edges are passivated or not. Differently, zigzag BNNRs with bare edges are magnetic and semiconducting due to presence of dangling edge bonds: the electrons are ferromagnetically coupled at the N edge while antiferromagnetically coupled at the B edge.[38] Upon edge passivation, zigzag BNNRs with two-side hydrogenated are nonmagnetic semiconductors, while those with one-side hydrogenated are ferromagnetic half-metals,[39] or antiferromagnetic *p*-type semiconductors (when only the B or N edges are selectively passivated).[40]

The common defects observed during BN growth are *N*-terminated triangle vacancies with missing B/N atoms.[41] Another important type of defect is Stone–Wales (SW) defect without any removed or added atom. The SW defect forms by rotating one B-N bond within four borazine rings by 90°, and reconstructing to form pentagon–heptagon pairs with appearance of new B-B and N-N bonds. There are two types of B-N bonds in perfect BNNRs (denoted as 1 and 2 in Figure 1(a) and 1(d)), and bond 1 or 2 can be rotated and rearranged into SW-1 or SW-2 defect, respectively. The formation of SW-2 defects is energetically preferred.

Our DFT studies show that introducing SW defects generates localized defect states and leads to band-gap reduction of armchair and zigzag BNNRs.[9] This finding is encouraging because it was generally believed that the band gap of BNNRs is rather robust. SW defect has been observed in graphene under electron beam irradiation; however, this defect has not been experimentally identified in BN, because energetically it is rather unfavorable to form homonuclear N-N or B-B bonds.

DFT computations revealed that molecular doping is also effective in tuning electronic structures of BN nanosystems.[10] The acceptor (tetracyanoquinodimethane, TCNQ) and donor (tetrathiafulvalene, TTF) molecules are noncovalently stacked on BN (Figure 2), and the optimized molecule-sheet distance (3.4–3.7 Å) is slightly larger than the interlayer space (3.3 Å) in layered *h*-BN. The interfacial charge transfer between TCNQ/TTF and BN causes significant band-gap narrowing of BN sheet/ribbons, resulting in *p*- or *n*-type semiconductors, respectively. The modifications of BN surface with patterned donor and acceptor molecules might be useful in the design of BN-based *p-n* junction devices and molecular electronics.
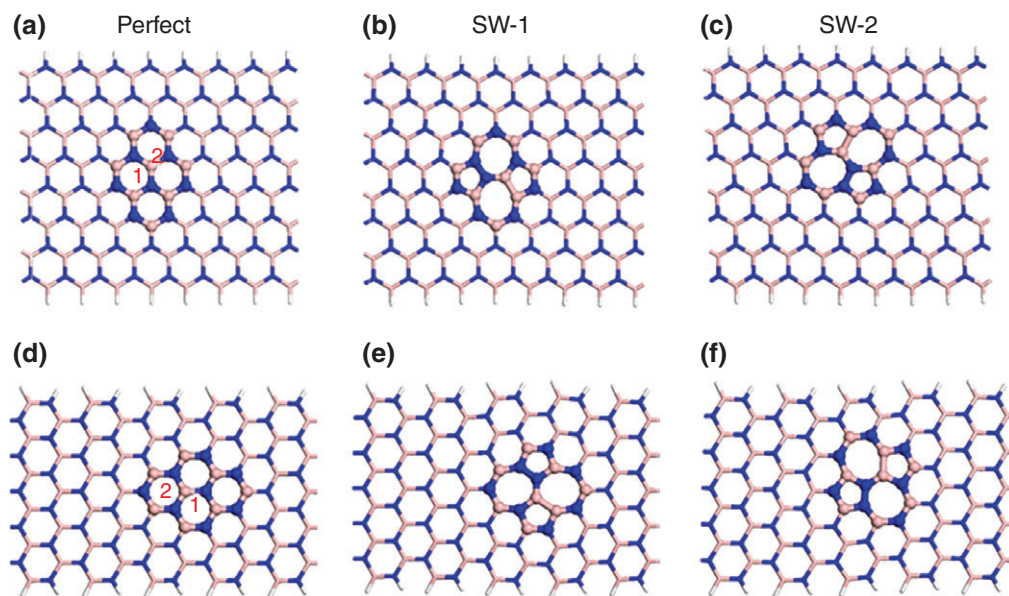
FIGURE 1 | Eight-zigzag (upper) and 11-armchair BNNRs (lower): (a, d) perfect and (b, e and c, f) with various SW defects. (Reprinted with permission from Ref 9. Copyright 2009 American Chemical Society)
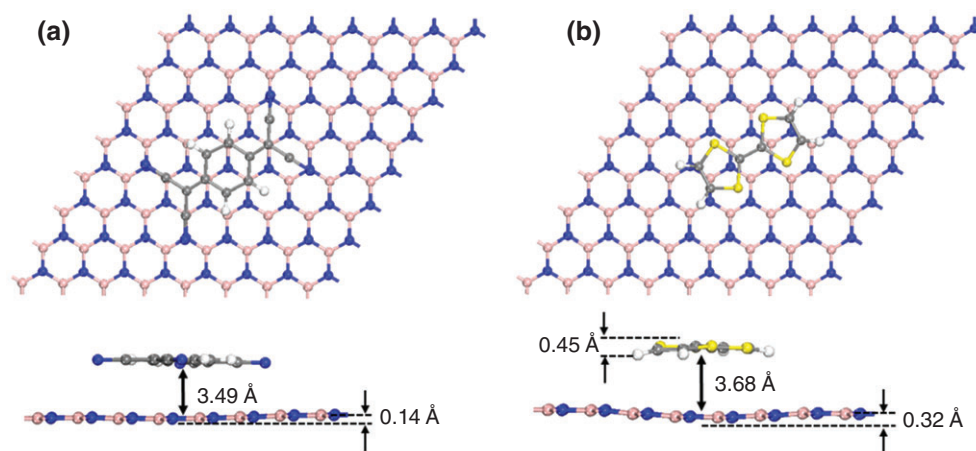
FIGURE 2 | Complexes of BN sheet with TCNQ (a) and TTF (b). (Reprinted with permission from Ref 10. Copyright 2011 American Chemical Society)

Surface covalent functionalization serves as another important tool for band-gap modification, and hydrogen is the typical modifier. Our computations revealed that hydrogenation induces different consequences on armchair and zigzag BNNRs.[11] Fully hydrogenated armchair BNNRs are nonmagnetic semiconductors, while fully hydrogenated zigzag counterparts are ferromagnetic metals. Interestingly, a gradual evolution from nonmagnetic semiconductors to ferromagnetic half-metals or metals can be realized by precisely controlling the hydrogenation coverage of zigzag BNNRs (Figure 3). A recent experimental study by Zhang et al. confirmed that few-layered BN exhibited a reduced band gap ($\sim$4.25 eV vs $\sim$5.6 eV) after hydrogen plasma treatment, although the exact degree of hydrogenation was unclear.[42]

Interlayer dihydrogen bonds can also theoretically tune band gaps of BN systems.[43] In chemistry, a dihydrogen bond is described as A-H$^{\delta+}\cdots^{\delta-}$H-B (A is a strongly electronegative atom such as O or N, while B is a less electronegative element than H such as B, Al), which is driven by the electrostatic attraction between two oppositely charged H. When hydrogenated BN bilayers are packed together, considerable interlayer B-H$^{\delta-}\cdots^{\delta+}$H-N dihydrogen bonds emerge. For chair-typed BN layers, such interactions drastically reduce the intrinsic large band gaps (from 3.27 eV for chair-like BN monolayer to 0.05 eV for bilayer) due to interfacial polarization and the resulting interlayer charge transfer. However, the lowest-energy configuration is not chair-typed, but stirrup-typed. The stirrup-like BN bilayer (band gap: 4.98 eV) preserves the insulating characteristic of stirrup-like BN monolayer (band gap: 4.92 eV), because there is negligible charge transfer between two interactive BN layers. Fortunately, the insulating band gap of more stable stirrup-typed bilayer BN can be engineered by applying external electric field. Similarly, another weak interaction, interfacial dihalogen bonding, can be also used for this purpose.[44]
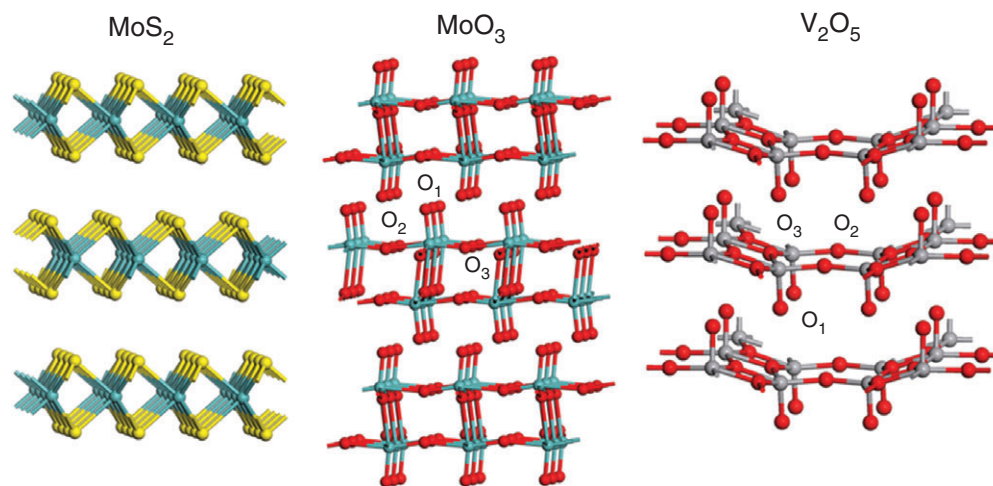
Nonplanar (MoS_2, MoO_3, and V_2O_5)

Layered MoS_2, α-MoO_3, and V_2O_5 are also assembled by weakly bonded layers. Unlike the one-atom-thick flat graphene and h-BN, monolayers of these materials have distinctive polyhedral-layer nonplanar geometries (Figure 4). Specifically, MoS_2 monolayer is organized in a hexagonal honeycomb structure consisting of Mo atom-layer sandwiched between two S atom-layers, each Mo(S) atom is coordinated to six (three) S(Mo) atoms forming trigonal prismatic coordination. Particularly, a single sheet of MoO_3 consists of a puckered bilayer, and the Mo atom centers a distorted octahedral coordination (MoO_6). Three crystallographically different oxygen atoms are present: surface terminal O1 and the bridge-connected twofold (O2) and threefold (O3) coordination O. V_2O_5 monolayer is built up of distorted VO_5 square pyramids that point upward and downward alternatively, and three inequivalent O sites (single-coordinated O1 and two- and three-coordinated bridging O2 and O3) also exist. Single layers of MoS_2, MoO_3, and V_2O_5 all have intrinsic band gaps.

MoS_2

MoS_2 is the most widely studied material among transition metal dichalcogenides (TMDs) due to its excellent properties and potential applications, particularly, in the next-generation nanoelectronic devices. The electronic property of MoS_2 is thickness-dependent. MoS_2 in its bulk form is an indirect band-gap semiconductor (1.29 eV). However, when the thickness is reduced down to one layer, the band gap
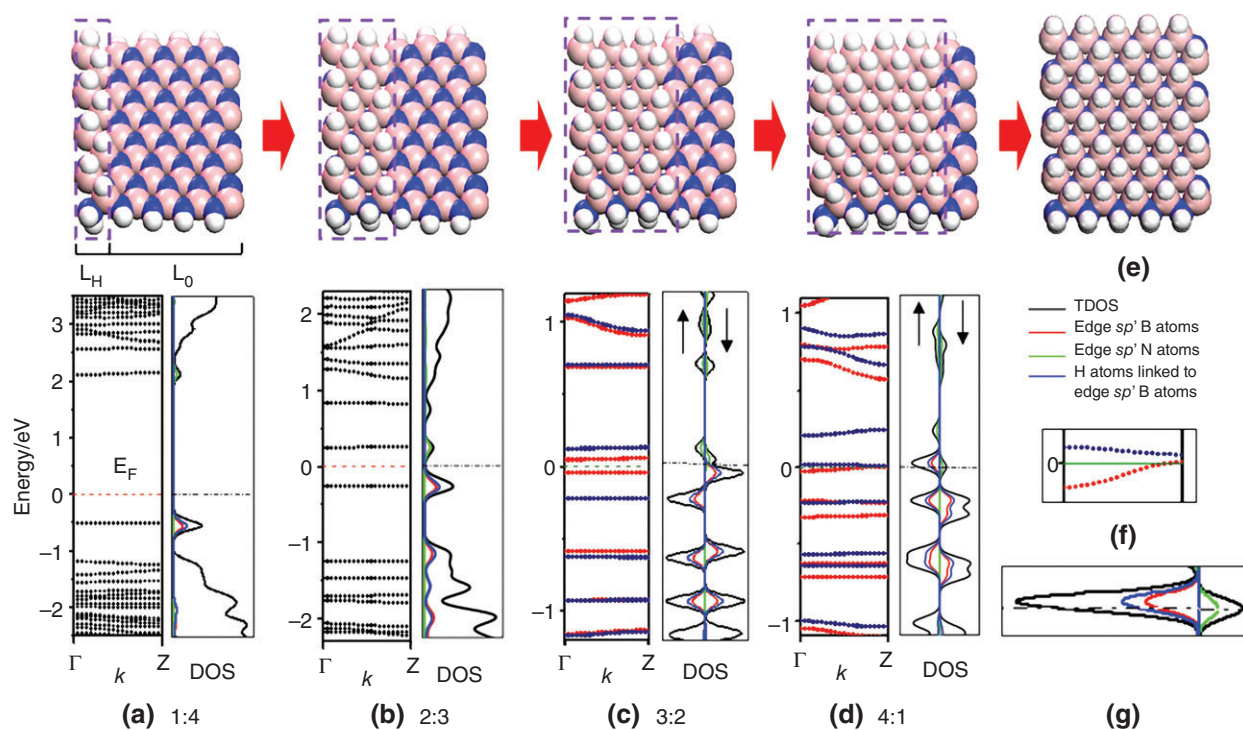
FIGURE 3 | Geometries and band structures of hydrogenated 8-zigzag BNNRs with $L_H : L_0$ ratios of (a) 1:4 (20%), (b) 2:3 (40%), (c) 3:2 (60%), (d) 4:1 (80%), and (e) 1:1 (100%). Parts f and g show zooms on the region about the Fermi level of band structure and density of states (DOS) of (d). (Reprinted with permission from Ref 11. Copyright 2010 American Chemical Society)


FIGURE 4 | Layered MoS_2, α-MoO_3, and V_2O_5.

is widened (1.90 eV) and transformed into a direct one.[45] The presence of a direct band gap in single-layer MoS_2 makes it extremely promising for optical applications. The medium band gap of single (few)-layer MoS_2 in the visible region also makes it attractive for fabricating field-effect transistors,[46] phototransistors,[47] and integrated circuits for logic applications.[2,3,48]

MoS_2 nanoribbons have also drawn considerable attention[49] (Figure 5). Depending on the cutting direction, two kinds of MoS_2 nanoribbons with armchair- ($AMoS_2$) or zigzag-shaped ($ZMoS_2$) edges can be generated, without considering edge saturation in earlier DFT studies. Different edge chiralities lead to distinct electronic properties. $AMoS_2$ nanoribbons are direct band-gap semiconductors with gaps converged to ~0.56 eV, which is smaller than that of the single-layer MoS_2 because of edge effects. Differently, $ZMoS_2$ nanoribbons are robustly ferromagnetic metals
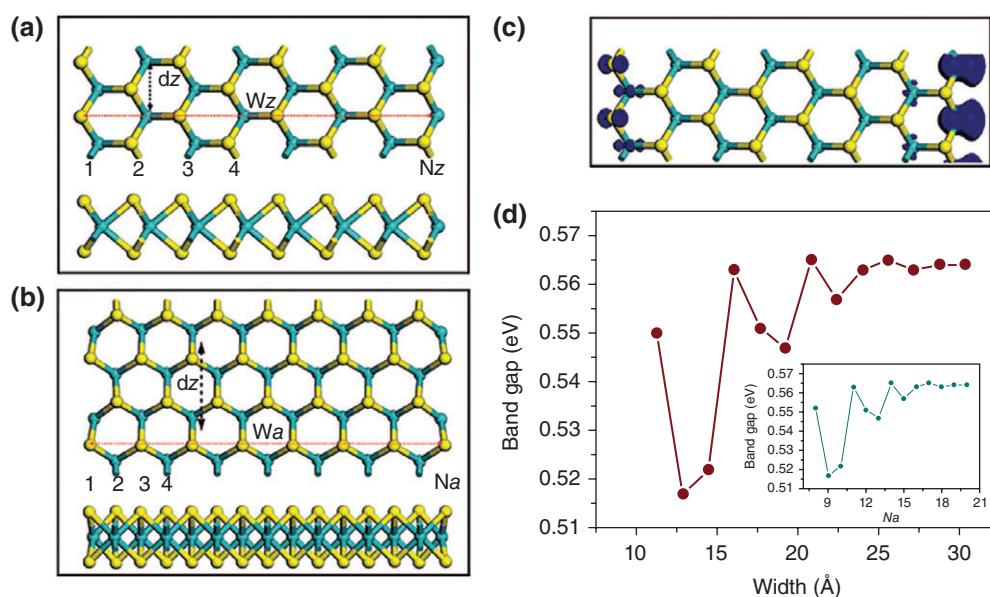
FIGURE 5 | Eight-zigzag (a) and 15-armchair (b) MoS_2 nanoribbons. Spin density distribution of 8-zigzag MoS_2 nanoribbon (c). Band-gap variation of armchair nanoribbons as a function of ribbon width (d) ($8 \leq N_a \leq 20$). (Reprinted with permission from Ref 49. Copyright 2008 American Chemical Society)

regardless of widths or thicknesses. The introduced magnetism mainly concentrates on edge Mo and S. In terms of structural stability, $ZMoS_2$ nanoribbons are energetically more preferable than $AMoS_2$ ones. Encouragingly, after our prediction, ultranarrow $ZMoS_2$ nanoribbons were successfully fabricated by Wang et al. via *in situ* growth inside carbon nanotubes.[16] Note that the bare Mo edge of $ZMoS_2$ nanoribbons is unstable, which prefers to be saturated by S, and later DFT studies by Erdogan et al.[50] showed that the electronic and transport properties of $ZMoS_2$ nanoribbons depend strongly on the edge passivation (full- or half-passivation with S).

A number of methods were theoretically proposed to control electromagnetic properties of MoS_2 systems, such as applying strains or electric fields,[51,52] adatom adsorption,[53] and vacancies.[54] In particular, an increase in external electric field perpendicular to MoS_2 bilayer narrows its indirect band gap continuously, and finally converts it to zero.[50] It was also found that single-layer MoS_2, which is typically nonmagnetic, attains a net magnetic moment upon adsorption of $3d$ transition metals such as Co, Cr, Fe, Mn, Mo, Sc, Ti, V, and W, as well as group 4A elements such as Si and Ge.[52] The creation of MoS_2 triple vacancies gives rise to significant magnetic moments, while monovacancies or divacancies do not induce magnetic moment.[53]

MoS_2 has many promising applications. Because of its tunable band gaps in the visible regions, MoS_2 can be applied to electronic and optoelectronic devices. MoS_2 is also promising as a catalyst or as an electronic sensor.[55] Moreover, its layered structure and facile formation of ion-intercalated state offer great opportunities to use MoS_2 as Li ion battery (LIB) materials. With this in mind, we explored Li adsorption and diffusion on different MoS_2 systems via DFT computations.[56] Li strongly binds to bulk MoS_2 with a moderate diffusion barrier. Reducing dimensionality into MoS_2 bilayer or monolayer significantly decreases Li diffusion barrier; however, the binding strength becomes slightly weaker. Owing to unique edge effects, cutting MoS_2 into zigzag nanoribbons remarkably enhances Li binding at the edges, and simultaneously preserves a high Li mobility with a low diffusion barrier. Regardless of the adsorption sites (Figure 6), Li would eventually migrate to edges by overcoming small activation barriers, which decrease progressively toward the edge. Therefore, compared with bulk and sheet-like MoS_2, MoS_2 nanoribbons should act as better LIB materials.

MoS_2 represents only one example of the TMD materials, many other 2D TMDs also attracted tremendous interest. Particularly, unlike the semiconducting property of MoS_2, VS_2 is electrically metallic. Our computations revealed that the intrinsic metallicity of VS_2 facilitates its performance as LIB anodes, and VS_2 monolayer is predicted to have higher Li storage capacity than MoS_2 or graphite.[57]

MoO_3
α-MoO_3 with orthorhombic symmetry is a layered oxide semiconductor well known as a redox solid
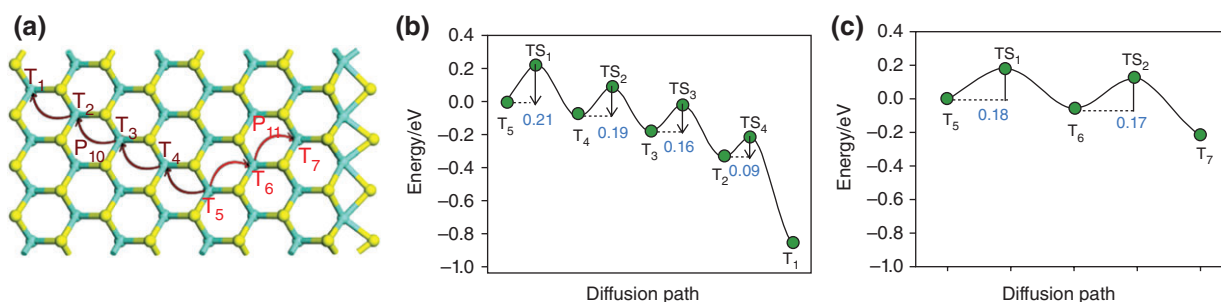
FIGURE 6 | (a) Two diffusion paths (P10 from T_5 to T_1, P11 from T_5 to T_7) on the basal plane of 8-zigzag MoS_2 nanoribbon. (b and c) Energy profiles for P10 and P11. (Reprinted with permission from Ref 56. Copyright 2012 American Chemical Society)

catalyst. α-MoO_3 comprises of a series of bilayers stacked along (010) plane (Figure 4). Its layered structure is particularly favorable for Li insertion, and has been widely studied as a LIB cathode material.[58] As a functional material, α-MoO_3 is also applied to photochromic devices,[59] photocatalytic reactions,[60] as well as gas and biosensors.[61]

Bulk α-MoO_3 has a wide-band gap (~3 eV), which results in low carrier concentration and is thus not suitable for the application to electronic devices. A range of approaches have been developed to tune its band gap, and one commonly adopted method is hydrogen intercalation. Insertion of H into α-MoO_3 layers produces H_xMoO_3, and theoretical studies showed that semiconducting α-MoO_3 shifts to metallic at H loading of $x > 0.25$.[62] Because of its high dielectric constant and easily tunable electronic properties, recent experiments have shown that α-MoO_3 emerges as an excellent oxide semiconductor for developing field-effect transistors with enhanced carrier mobility.[26]

Our DFT computations also indicated that the electronic properties of MoO_3 sheets can be alternatively tuned by cutting into nanoribbons, modifying with hydrogenation or applying strain.[63] The derived MoO_3 nanoribbons can be nonmagnetic semiconductors, magnetic semiconductors, or magnetic metals depending on the cutting patterns, among which the nonmagnetic semiconducting nanoribbons have higher stability. The semiconducting single-layer MoO_3 is transformed into a ferromagnetic metal when surface O1 and O2 atoms are saturated by H. Regardless of edge shapes and widths, all the edge-hydrogenated MoO_3 nanoribbons are nonmagnetic semiconductors, whereas all the fully hydrogenated MoO_3 nanoribbons (both surface and edge are hydrogenated) are ferromagnetic metals. The induced magnetism mainly originates from $4d$ orbitals of Mo atoms. The above predictions are consistent with experimental findings of band-gap reduction of MoO_3 sheets upon hydrogenation[26] and enhanced electronic transport of H_xMoO_3 nanobelts.[64] Besides hydrogenation, the band gaps of

MoO_3 sheet/ribbons can be tuned by exerting axial strain, and their nonmagnetic semiconducting characters remain unchanged within 10% tensile or compressive forces.
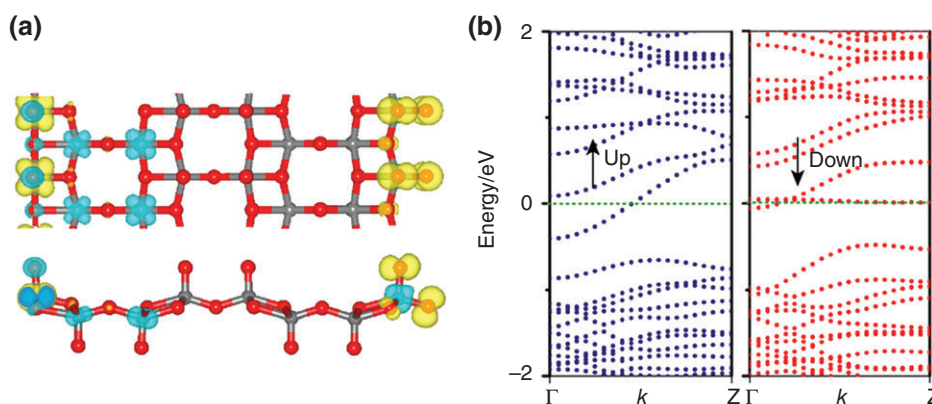
V_2O_5

V_2O_5 also crystallizes in an orthorhombic structure comprising layers of distorted [VO_5] square pyramids stacking along (001) direction (Figure 4).

Bulk V_2O_5 has a band gap of ~2.4 eV, and the (001) monolayer has similar physical properties and stability to its bulk. Our DFT investigations demonstrated that single-layer V_2O_5 sheet and nanoribbons possess tunable properties.[65] Single-layer V_2O_5 behaves as a nonmagnetic semiconductor (indirect gap: 1.91 eV). Surface hydrogenation transforms V_2O_5 into a ferromagnetic metal. Note that theoretical studies by Negreira et al. showed that surface oxygen defects would decrease the band gap of V_2O_5 (001) layer, and a semiconductor-to-metal transformation occurs with the addition of oxygen vacancies.[66] Zigzag V_2O_5 nanoribbons are intrinsically magnetic metals with considerable bands crossing the Fermi level in both minority and majority spin channels (Figure 7), and the generated magnetism mostly comes from the unfilled d orbitals of edge V. Armchair nanoribbons are nonmagnetic semiconductors with direct gaps around 1.82 ~ 1.88 eV. Both types of nanoribbons become nonmagnetic semiconductors when only edge atoms are hydrogenated, and are further transformed into half-metals when surface and edge atoms are completely hydrogenated. These tunable properties lead to possible applications of V_2O_5 nanostructures to the fields of nanoelectronics and spintronics.

Scaling V_2O_5 to nanoscale dimensions endows them with great potentials for important applications. Like layered MoS_2 and MoO_3, 2D layered V_2O_5 sheets have been extensively studied as high-capacity cathode materials for LIBs. According to Rui et al.'s experimental report, single-layered and few-layered V_2O_5 nanosheets showed better electrochemical

FIGURE 7 | (a) Spin density distribution (top and side views), and band structure (b) of 12-zigzag V_2O_5 nanoribbon. (Reprinted with permission from Ref 65. Copyright 2011 American Chemical Society)

performances than bulk phase, due to high active-specific surface area and shortened Li insertion/extraction pathways provided by the ultrathin thickness.[67,68] V_2O_5 has also been widely used as a catalyst, and DFT studies revealed that V_2O_5 monolayer could promote the dehydriding kinetics in MgH_2, which facilitates the development of Mg-based hydrogen storage materials.[69]

Besides the above focused h-BN, MoS_2, α-MoO_3, and V_2O_5, there are many more vdW materials,[2] and these materials (some of them have not been exfoliated in experiments) with diverse ranges of properties yield a rich set of novel 2D systems to explore.

GRAPHENE-LIKE MATERIALS ACHIEVED FROM INORGANIC MATERIALS WITH STRONG INTERLAYER INTERACTIONS

The above h-BN, MoS_2, α-MoO_3, and V_2O_5 belong to layered vdW solids, and then here a question arises: can graphene-like materials be achieved in layered materials with strong (covalent or ionic) interactions between their layers? Actually, there are a few successful examples in obtaining thin nanosheets of strongly connected inorganic materials, such as ZnO and $M_{n+1}AX_n$.

From Wurtzite Phase (ZnO) to Graphitic Layers

Wurtzite materials occur widely in most II–VI and III–V binary compounds. In Wurtzite structures, alternating hexagonal planes are interconnected by strong covalent bonds, and all atoms are in sp^3 hybridization. Particularly, cutting Wurtzite crystal along c axis leads to polar (0001)-oriented films with a cation-terminated surface on one side and an anion-terminated surface on the other side. Such polar surfaces are intrinsically unstable due to divergence of surface energy. Freeman et al. predicted that polar (0001)-oriented ultrathin films of Wurtzite materials undergo an interesting structural transformation into layered graphitic structures.[12] In graphitic structures, each atom goes from tetra-coordination to planar tri-coordination, and surface polarity is completely removed, structurally similar to graphene. As an example, Wurtzite ZnO nanosheets with limited Zn-O bilayers are relaxed to graphite-like structures[70] (Figure 8(a)). The observed transition is accompanied by Zn-O bond contraction within each bilayer and interlayer distance expansion. Graphitic ZnO nanosheets are semiconductors because of surface-state depolarization, with band gaps reduced with increasing thickness, and then converged to a thickness-independent value of 2.05 eV (Figure 8(b)). This appealing prediction on Wurtzite-graphite transition was confirmed by an epitaxial-growth experiment, wherein two-monolayer-thick planar ZnO(0001) films were observed on Ag substrates.[15]

The electronic structures of graphite-like ZnO can be additionally modulated by adatom adsorption of H[69] or F[71]. Hydrogen or fluorine saturation of surface atoms can transform these graphitic ZnO nanosheets into Wurtzite configurations, and their electronic and magnetic properties depend on H or F adsorption sites and sheet thickness.

In addition to ZnO, the thin nanofilms of many other Wurtzite materials (such as SiC, BeO, ZnS, AlN, and GaN) with polar (0001) surfaces are also found to form graphitic-like structures[12,72,73]; however, so far these graphitic systems remain hypothetical in theory.

From MAX Phase to MXene

'MAX' phase is a family of layered ternary metal carbides, nitrides, or carbonitrides with a $M_{n+1}AX_n$ (n =
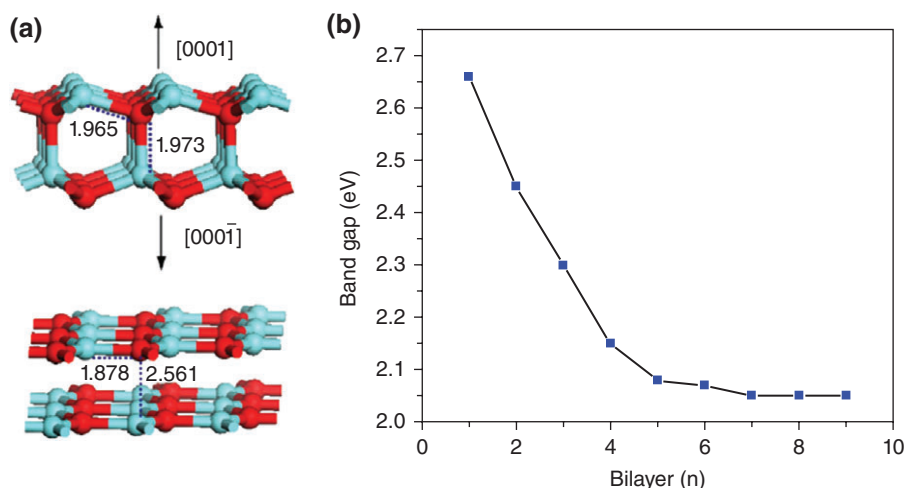
FIGURE 8 | (a) Two-bilayer ZnO nanosheets with initial Wurtzite structure and optimized graphitic structure. (b) Band-gap evolution of graphitic nanosheets as a function of bilayer number, n ($1 \le n \le 9$). (Reprinted with permission from Ref 70. Copyright 2010 American Chemical Society)

1, 2, 3) formula. Depending on the combination of M (Ti, Sr, V, Cr, Ta, Nb, Zr, Mo, or Hf), A (III A or IV A), and X (C and/or N), MAX occurs in more than 60 different categories. MAX combines the physicochemical properties of both metals and ceramics, and possesses unique properties, such as remarkable machinability, excellent oxidation resistance, and high electrical and thermal conductivity, leading to various industrial applications. MAX adopts hexagonal structures with *P*63/mmc symmetry, consisting of alternative stacking of MX layers and planar A atomic layers (Figure 9). The MX layers are held together by interleaved A layers via partially ionic bonding, and thus separating MX layers cannot be easily realized.

Amazingly, the formidable task to exfoliate MX layers was accomplished by a rather simple but effective approach. Gogotsi's group selectively extracted A layers by acid treatment (HF acid), and then used liquid-phase ultrasonication to facilitate the exfoliation into 2D MX layers. Through this method, many MX layers such as Ti_3C_2, Ti_2C, Ta_4C_3, TiNbC, $(V_{0.5}Cr_{0.5})_3C_2$, Ti_3CN_x (x < 1), Nb_2C, and V_2C have been successfully isolated from their Al-containing MAX phases.[74–76] Depending on the concentration of HF solution, the surfaces of these layers are usually functionalized by F or/and OH groups. These exfoliated carbide or carbonitride nanosheets are termed as 'MXene', to signify the loss of A element and emphasize these materials' graphene-like 2D morphology.

The electronic properties of MXenes can be tuned by changing compositions and their surface terminations, which have been widely studied via DFT computations. For example, bare Ti_3C_2, built up of quintuple layers stacked in Ti(1)-C-Ti(2)-C-Ti(1) sequence (Figure 10(a)), is featured as a magnetic metal. Its
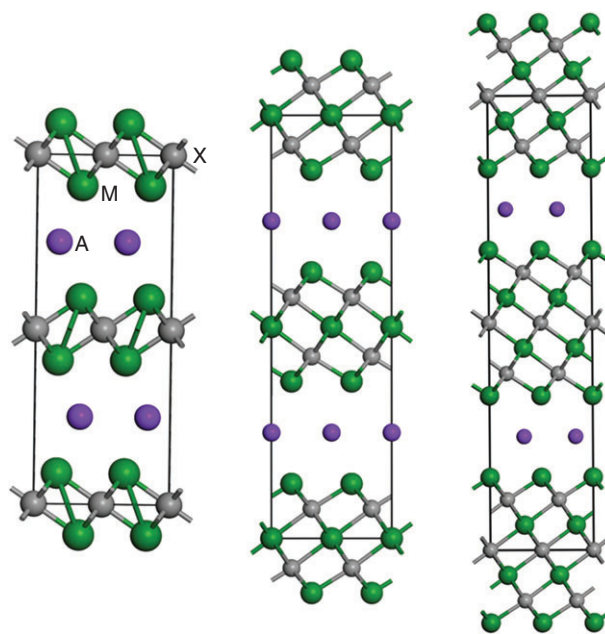
FIGURE 9 | Structures of M_2AX, M_3AX_2, and M_4AX_3.

induced magnetism originates from delocalized dangling 3*d* orbitals of surface Ti atoms. Upon surface termination, the unsaturated surface Ti atoms form strong bonds with attached functional groups, and the derived $Ti_3C_2F_2$ and $Ti_3C_2(OH)_2$ become nonmagnetic semiconductors with small band gaps around 0.04–0.07 eV.[77]

Other types of MXenes, M_2C (M = Sc, Ti, V, Cr, Zr, Nb, or Ta) and M_2N (M = Ti, Cr, or Zr) with bare surfaces are also metallic.[78] When their surfaces are functionalized by F, OH, or O, the as-functionalized MXenes are metallic except for Sc_2CF_2, $Sc_2C(OH)_2$,
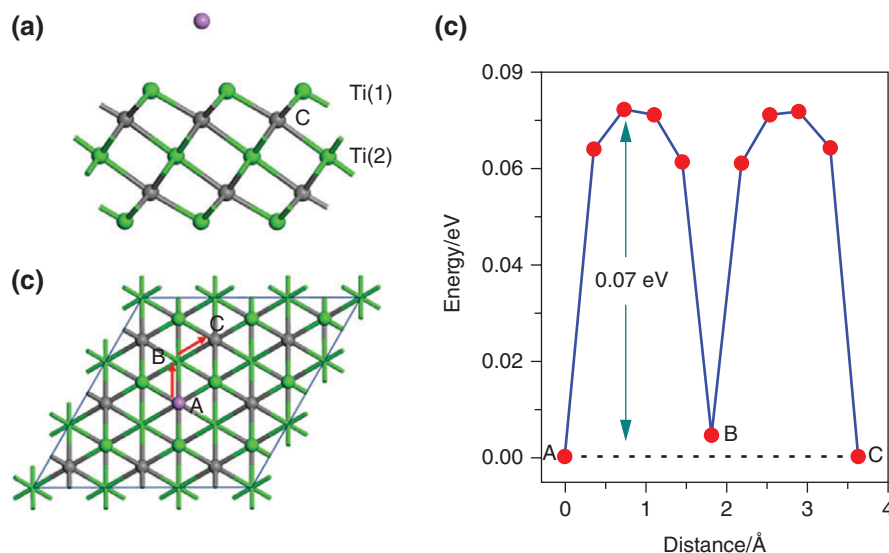
FIGURE 10 | (a) Side view of Li-adsorbed Ti_3C_2. (b) Top view of the lowest-energy migration pathway (A–B–C) for Li diffusion on Ti_3C_2. (c) Diffusion barrier profile. A, B, and C represent ontop C, ontop Ti(2), and ontop C sites. (Reprinted with permission from Ref 77. Copyright 2012 American Chemical Society)

Sc_2CO_2, Ti_2CO_2, Zr_2CO_2, and Hf_2CO_2, which are semiconductors with band gaps between 0.25–2.0 eV.[79] Thicker MXenes ($Ti_{n+1}C_n$ and $Ti_{n+1}N_n$, where n = 4–9) with both bare and functionalized surfaces are all predicted to be metallic.[77]

In addition to the extensive theoretical predictions, the electrical conductivities of some free-standing MXene discs (Ti_2C, $TiNbC$, Ti_3CN_x, Ta_4C_3, or Ti_3C_2) have also been experimentally measured, which are comparable to those of multilayered graphene.[74]

The rich chemistries and unique electronic properties endow MXenes with many promising applications. We performed DFT studies on one representative MXene, Ti_3C_2, in terms of its Li storage capability[76] (Figure 10). Li adsorption forms strong coulombic interaction with Ti_3C_2 host (Li prefers to adsorb onto C atoms), and the adsorbed Li becomes partially ionized due to large charge transfer between Li and MXene. In regard to the diffusion properties, bare Ti_3C_2 exhibits the lowest diffusion barrier (0.07 eV) and highest Li storage capacity (320 mAh g^{-1}, up to $Ti_3C_2Li_2$ stoichiometry) as compared with its fluorinated and hydroxylated derivatives. The higher diffusion barriers on $Ti_3C_2F_2$ and $Ti_3C_2(OH)_2$ are ascribed to steric hindrances induced by surface groups. For a better implementation of MXene into advanced Li ion batteries, an ideal surface without functionalization would be desirable, although this would be synthetically difficult to achieve. Moreover, Ti_3C_2 is found to have a low operation voltage (0.62 eV) during Li-ion intercalation, which, when combined with its good electrical conductivity, and low diffusion barrier, renders Ti_3C_2 strong potential as LIB anodes.[80]

The performances of several MXenes (Ti_2C, Ti_3C_2, V_2C, or Nb_2C) as LIB anodes have been tested in recent experiments.[75,81] In general, these MXenes showed excellent Li-ion capacity at extremely high rates. MXenes also showed great promise as electrode materials for supercapacitors.[82,83] A variety of cations (Li^+, Na^+, K^+, or NH_4^+) can readily intercalate into Ti_3C_2 layers, which offer higher volumetric capacitance than porous carbon electrical double-layer capacitors. Moreover, MXenes were also experimentally found to be promising catalyst supporters to enhance oxygen reduction reaction activity.[84]

The discovery of MXenes greatly expands the family of 2D nanomaterials. However, to date, only a limited number of MXenes were experimentally produced. As the exfoliation technique increases in effectiveness, more MXenes would be exfoliated from their MAX precursors, and diverse properties as well as numerous applications are expected.[85–91]

COMPUTATIONAL DESIGN OF NOT-YET-SYNTHESIZED GRAPHENE-LIKE MATERIALS WITH NOVEL CHEMICAL BONDING (B_2C, SiC_2, BSi_3, ARSENENE, AND ANTIMONENE)

Carbon can have sp, sp^2, or sp^3 hybridized states. Silicon is in the same column of the periodic table as carbon; however, Si ordinarily prefers sp^3 hybridization.

Attempts to design molecules and materials with novel chemical bonding such as planar tetracoordinate C (ptC) or Si (ptSi) have been hotly pursued since the initial seminal work on the possible existence of ptC by Hoffmann.[92] Various ptC- or ptSi-containing molecules have been designed, which are beyond the scope of our current review. Herein, we focus on two hypothetical graphene-like materials containing ptC and ptSi based on computational predictions.

B_2C

B_2C sheet (Figure 11(a)–(c)), as proposed by Wu et al., is based on a predicted ptC molecule 'CB$_4$', and is essentially a 2D extended network of C_{2v}–CB$_4$ motif.[13] B_2C consists of closely packed hexagons and rhombi, and each C is bonded with four B atoms, forming tetracoordination C moiety. B_2C is not completely planar as the CB$_4$ molecule, but is slightly corrugated with a tiny separation of B-layer and C-layer by ~0.085 Å, because the B/C ratio in B_2C is lower than that in CB$_4$ molecule, and the reduced B/C ratio leads to more valence electrons in $2p$ orbitals. B_2C has excellent mechanical, thermal, and chemical stability, which can maintain structural integrity up to 2000 K.

Electrically, B_2C sheet and its derived nanoribbons are all rigorous metals.

As a hypothetical material, the 2D B_2C monolayer is predicted to possess many intriguing properties. Based on first-principles lattice dynamics and electron-phonon coupling computations, the B_2C sheet is predicted to be an intrinsic 2D superconductor with a relatively high transition temperature in the range of 14.3–19.2 K.[93] Because of its electron-deficient character, the hexagonal hollow site of the B_2C sheet can strongly hold metal atoms such as Li[94] and Ti.[95] The attached metals donate their s electrons to B_2C leading to partially filled B p and C p orbitals, and meanwhile the B_2C back-donates some electrons to the low-lying Li p or Ti d orbitals, resulting in strong hybridizations between Li (Ti) and the B_2C substrate. The metal-doped B_2C can adsorb hydrogen molecules with moderate binding energies and high gravimetric density, thus can be potentially developed for hydrogen storage applications.

SiC_2

Stimulated by Wu et al.'s study on B_2C, we designed an interesting SiC_2 where ptSi is stably embedded into a periodic 2D network[14] (Figure 11(d)). SiC_2 is designed
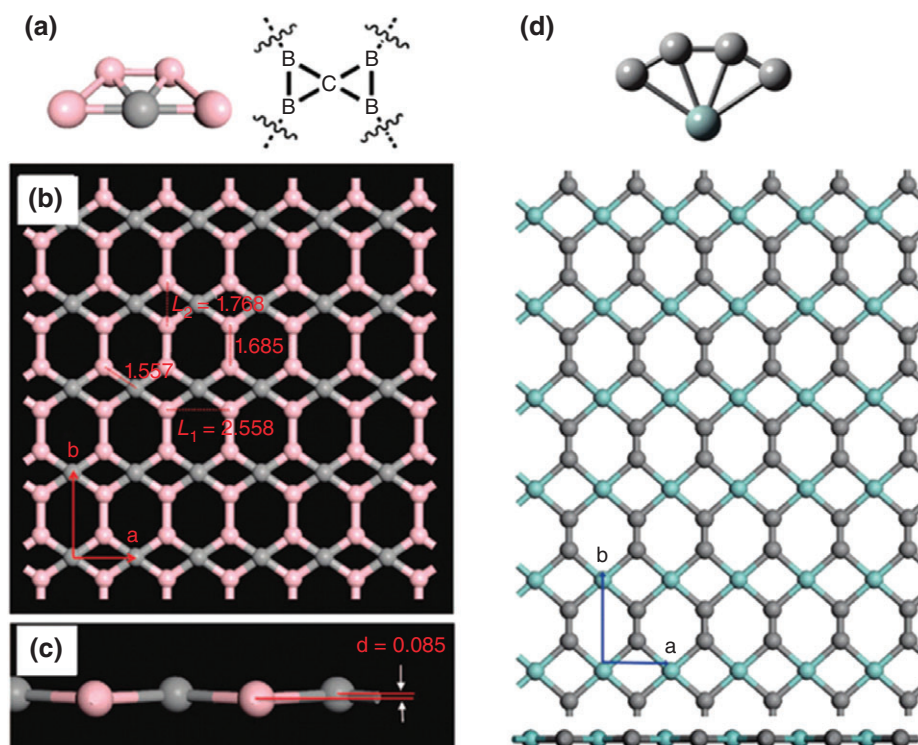
FIGURE 11 | (a) CB$_4$ molecule (left) and a C_{2v}–CB$_4$ motif (right); (b) Top and (c) side view of B_2C. (Reprinted with permission from Ref 13. Copyright 2009 American Chemical Society). (d) SiC$_4$ molecule (upper) and SiC_2 (lower). (Reprinted with permission from Ref 14. Copyright 2011 American Chemical Society)

based on a planar SiC_4 molecule. In SiC_2, the Si-C bond is slightly longer than typical Si-C single bond, while the C-C bond is featured as a typical C=C bond. One C=C bond and its four bonding Si atoms resemble the structure of ethylene. The planarity-preferred ethylene-like skeletons act as a driving force to yield a perfectly planar SiC_2 network. SiC_2 is a stable phase, being a local minimum at the potential energy surface, and possessing high kinetic stability up to 800 K. Similar to B_2C, all ptSi-containing nanostructures, ranging from SiC_2 sheet and nanoribbons to nanotubes, are robustly metallic. The characteristic metallicity is governed by π-type C=C bonds.
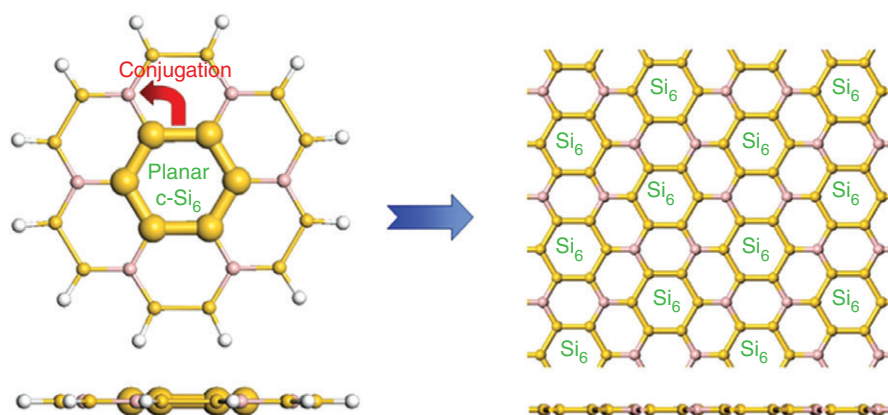
BSi_3 Silicene

Benzene and graphene are the two paradigms of Hückel-aromatic molecules and 2D aromatic networks consisting of planar aromatic D_{6h} cyclic six-membered carbon ring(s) (c-C_6). However, the relatively weak π bonding ability of Si versus C makes the silicon analogues of benzene and graphene (hexasilabenzene molecule and 2D silicene sheet, respectively) favor the low-buckled honeycomb structure. Thus, searching for an effective strategy to stabilize the planar aromatic D_{6h} cyclic six-membered silicon ring (c-Si_6) becomes an intriguing project for chemists. By combining DFT optimizations and global minimum search based on particle swarm optimization (PSO) method, Tan et al.[96] found that replacing the Si atoms surrounding the central c-Si_6 in the silicon analogue of coronene with B ($B_6Si_{18}H_{12}$) can significantly stabilize the planarity of the central c-Si_6 ring, which is attributed to the strong π-p conjugation between c-Si_6 and B atoms (Figure 12). Extending this $B_6Si_{18}H_{12}$ model to 2D network led to planar c-BSi_3 silicene sheet, which can be viewed as B-substituted silicene. Electronic structure

computations indicated that c-BSi_3 silicene is a typical metal, which is electrically robust to mechanical strain and surface chemical functionalization. The intrinsically metallic c-BSi_3 is predicted to have high lithium storage capability (1410 mA·h/g for single-layer c-BSi_3 and 846 mA·h/g for double-layer c-BSi_3) and low diffusion barrier (below 0.6 eV).[97] This indicates that c-BSi_3 silicene could be potentially explored as an anode materials for LiBs with high capacity and fast charge/discharge rate.

Arsenene and Antimonene (As and Sb Monolayer)

The group-V mono-elemental crystals such as bulk gray As and Sb form a layered honeycomb structure-like graphite. However, the As and Sb layers adopt buckled structures with single-layer thickness of about 1.35 Å (Figure 13), similar to the buckled silicene and germanene. Recently, Zhang et al.[98] predicted that the As and Sb monolayers have strong kinetic stability (no soft phonon modes are available in the computed phone dispersion spectra) and high feasibility for experimental realization. In fact, each As or Sb atom with five valence electrons bonds to three adjacent atoms, which endows them with octet stability. Interestingly, although bulk As and Sb are semimetals, they are transformed into indirect semiconductors with band gaps of 2.49 and 2.28 eV when thinned to monolayers. The weakening in interlayer interaction with the decreased layered thickness as well as the quantum confinement effect would most likely contribute to the semimetal to wide-band-gap semiconductor transition in the As/Sb systems. The computed effective mass of electron for As and Sb monolayer is smaller than that of monolayer MoS_2, indicating that As and Sb monolayer would exhibit high carrier mobility. More

FIGURE 12 | Top and side view of the $B_6Si_{18}H_{12}$ molecule (left) and the extended 2D c-BSi_3 silicene (right). (Reprinted with permission from Ref 96. Copyright 2014 American Chemical Society)
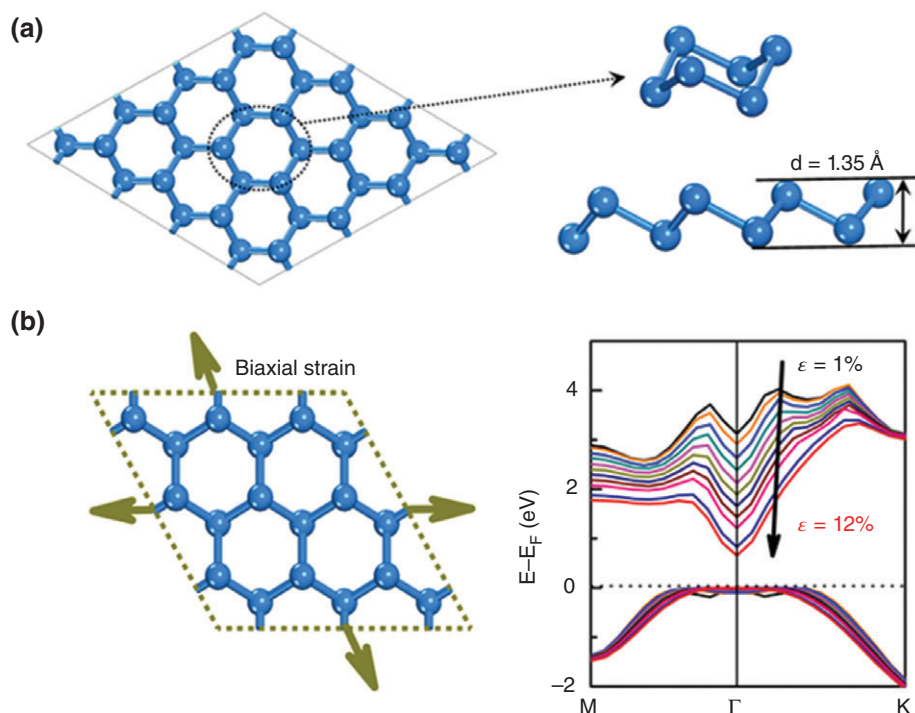
FIGURE 13 | (a) Side- and top-view structures of wrinkling As monolayer (arsenene). (b) (left) The schematic arsenene under biaxial tensile strain; (right) The changes of the top of valence band and bottom of conduction band of the arsenene with increasing biaxial tensile strain. (Reprinted with permission from Ref 98. Copyright 2015 John Wiley and Sons)

interestingly, both As and Sb monolayers further undergo an indirect to direct band-gap transition upon applying biaxial strain. The dramatic electronic structure changes would open up their possibilities for applications in high-speed transistors, blue/UV optoelectronic devices, and mechanical sensors based on 2D As and Sb nanosheets.

GRAPHENE-LIKE CPs

CPs are inorganic–organic hybrid materials constructed with organic linkers and metal ions. A rich variety of architectures and dimensionalities can be achieved by suitable selection of the building blocks. Particularly, 2D CPs with single-layer thickness represents a novel class of atomically regular 2D materials beyond graphene, and some of them have been generated by unique experimental techniques. Amo-Ochoa et al. isolated single-layer $[Cu_2Br(IN)_2]_n$ (IN = isonicotinato) from its layered crystal via liquid-phase sonication.[99] In $[Cu_2Br(IN)_2]_n$, each Cu dimer bridged by bromine is coordinated by four oxygen atoms from two IN units and two nitrogen atoms from the other two IN ligands, making each Cu adopt trigonal-bipyramidal coordination geometry. Abel

et al. realized polymeric Fe-phthalocyanine (poly-FePc) sheet by coevaporation of Fe and 1,2,4,5-tetracyano-benzene.[100] The poly-FePc with square symmetry can be seen as embedding of transition metals into the regular pores of planar phthalocyanine sheets, where the macrocyclic N groups offer the coordination sites. Kambe et al. synthesized π-conjugated nickel bis(dithiolene) nanosheet ($[Ni_3C_{12}S_{12}]_n$) via polymerization between benzenehexathiol and $Ni(OAc)_2$.[101] This organometallic sheet is inherently cross-linked by Ni-S covalent bonds forming square-planar Ni-S coordination, and such a framework with hexagonal symmetry is perfectly planar. Note that unlike the in-plane covalent bonds in other 2D systems, the coordination bonds between metal ions and ligands in CPs are much weaker.

Interesting properties and multifunctional applications of single-layer CPs were predicted via DFT computations, and the unique functions mainly arise from unsaturated metal centers as well as the organic ligands. Although each $[Cu_2]^{3+}$ dimer in $[Cu_2Br(IN)_2]_n$ possesses one unpaired electron, the extended $[Cu_2Br(IN)_2]_n$ favors antiferromagnetic dimer-coupling, and is semiconducting with a band gap of 0.47 eV. $[Cu_2Br(IN)_2]_n$ has strong tendency to adsorb NO and NO_2, stronger than H_2, O_2, CO, CO_2, N_2, and

NH$_3$. They are chemisorbed with large adsorption energies (~1 eV) and can sensitively modify the electronic properties of [Cu$_2$Br(IN)$_2$]$_n$. This suggests its potential application as NO or NO$_2$ molecular sensors[102] (Figure 14).

The poly-FePc nanosheet is predicted to be an antiferromagnetic semiconductor. Interestingly, a ferromagnetic half-metal would be realized when replacing Fe centers with Mn.[103] Poly-MnPc displays metallic d_{xz} and d_{yz} orbitals that hybridize with p electrons of Pc, which mediates the long-range ferromagnetic coupling. The Curie temperature of poly-MnPc is predicted to be ~150 K, quite comparable to the highest one achieved in Mn-doped GaAs.

The metal-phthalocyanine porous sheets have many potential applications. The presence of regularly and separately spaced transition metal atoms in the polymer lattices generates peculiar and tunable magnetic properties, which are interesting for spintronics applications. Moreover, the uniformly embedded metal atoms also generate intriguing gas adsorption and catalytic properties. For instance, the poly-ScPc sheet is predicted to be able to effectively capture CO$_2$ molecules, which shows high selectivity for CO$_2$ as compared with H$_2$.[104] The single-layer poly-CoPc sheet is found to be a promising high-activity nanocatalyst for CO oxidation.[105]

Nickel bis(dithiolene) 2D polymers also demonstrate attractive properties. Such a sheet behaves as a nonmagnetic indirect-band-gap semiconductor, and its lowest conduction band comes from unoccupied p_z orbitals of S atoms, making S atoms accept electrons from the occupied p_z orbitals. Indeed, our computations verified that nickel bis(dithiolene) shows high cycloaddition reactivity with ethylene, where they react to form *cis*-interligand S,S′-adducts[106] (Figure 15). When an extra electron is added, the adduct becomes destabilized and spontaneously dissociates into

ethylene and nickel bis(dithiolene) anion. Therefore, ethylene would controllably bind to or release from nickel bis(dithiolene) in neutral and reduction condition, respectively, making nickel bis(dithiolene) a prospective electrocatalyst for olefin purification. Besides, this 2D nickel bis(dithiolene) framework is predicted to be a 2D organic topological insulator with unique quantum transport properties.[107,108] This brings in great potential for using this organometallic polymer in spintronics and quantum computing.

Coordination polymers are an intriguing class of 2D porous materials, which allow elaborate and flexible control over the porosity, composition, and functionality through proper structural design. Although layered CPs can be easily synthesized from the perspective of chemists, substantial challenges remain for the realization of single-layer CPs. Achieving isolated single sheets of CPs with unique functionalities is an ongoing but challenging target.

CONCLUSION

The recent blossoming of graphene has initiated tremendous interest in exploring graphene-like materials. In this review, we survey recent progress in the DFT computational investigations on various graphene-like 2D materials, in which most of them have access to experimental support, while a few of them are still hypothetical in theory. We mainly devote ourselves to predicting the fundamental electronic and magnetic properties, and exploring their technical potentials. Our studies only cover a small part of the large family of noncarbon graphene-like materials, and there are many more for our adventure in this rapidly rising area. Many opportunities and challenges exist. For instance, synthesizing graphene-like nanosheets or nanoribbons with desired thicknesses or edges and improving their
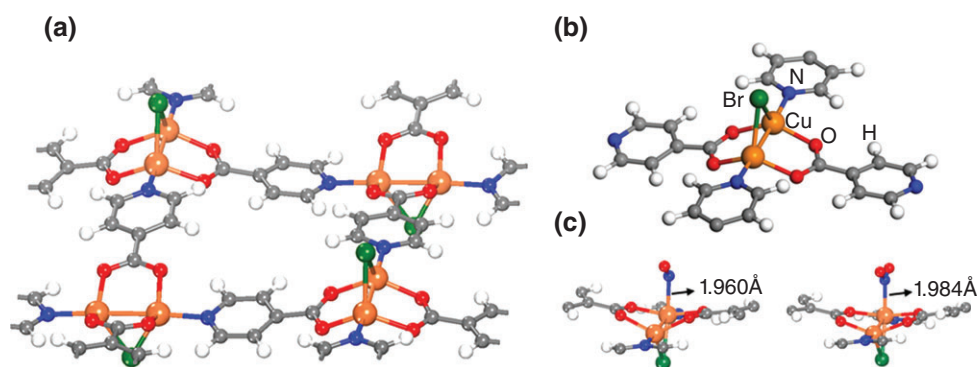
FIGURE 14 | (a) [Cu$_2$Br(IN)$_2$]$_n$ and (b) [Cu$_2$]$^{3+}$ coordination environment. (c) Adsorption of NO and NO$_2$ on [Cu$_2$Br(IN)$_2$]$_n$, only geometry around metal sites is shown. (Reprinted with permission from Ref 102. Copyright 2012 American Chemical Society)
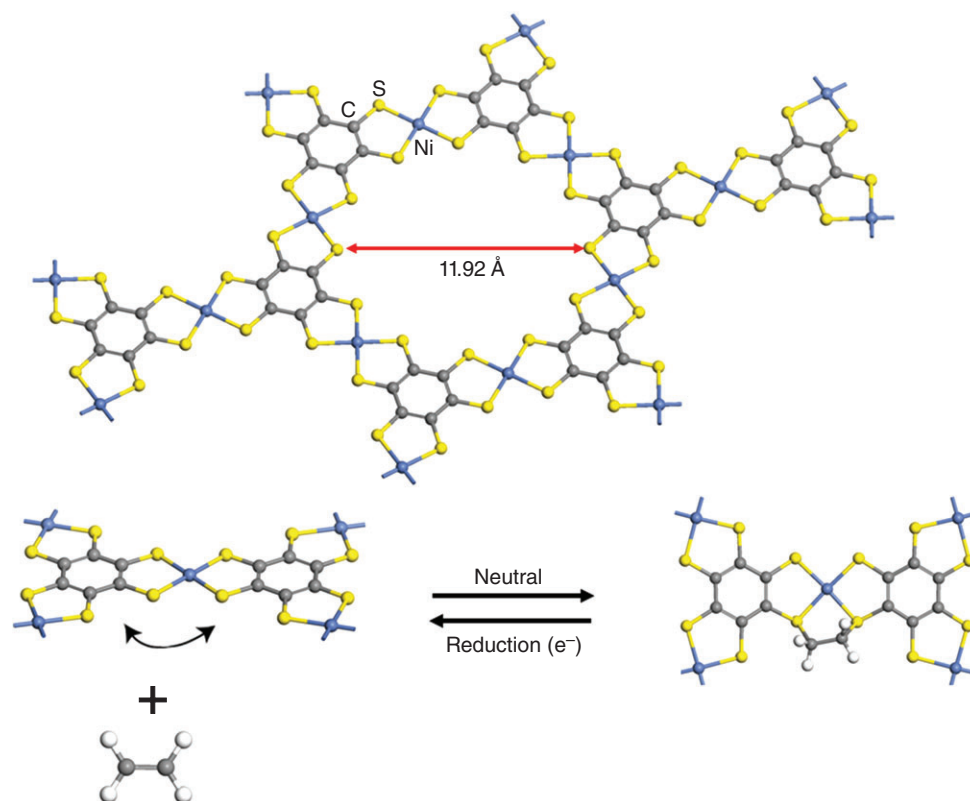
FIGURE 15 | Nickel bis(dithiolene) nanosheet (upper), and schematics of its addition with ethylene (lower). (Reprinted with permission from Ref 106. Copyright 2013 American Chemical Society)

structural qualities are experimentally demanding. Many prospects of graphene-like materials, such as basic physical and chemical properties, and electronic structure tuning, remain open to further explorations.

The fundamental investigations and technological applications of graphene-like materials are still in its very infancy, and they deserve more computational and experimental efforts in the near future.

ACKNOWLEDGMENT

REFERENCES

1. Novoselov KS, Geim AK, Morozov SV, Jiang D, Zhang Y, Dubonos SV, Grigorieva IV, Firsov AA. Electric field effect in atomically thin carbon films. *Science* 2004, 306:666–669.

2. Tang Q, Zhou Z. Graphene-analogous low-dimensional materials. *Prog Mater Sci* 2013, 58:1244–1315.

3. Xu M, Liang T, Shi M, Chen H. Graphene-like two-dimensional materials. *Chem Rev* 2013, 113:3766–3798.

4. Koski KJ, Cui Y. The new skinny in two-dimensional nanomaterials. *ACS Nano* 2013, 7:3739–3743.

5. Song X, Hu J, Zeng H. Two-dimensional semiconductors: recent progress and future perspectives. *J Mater Chem C* 2013, 1:2952–2969.

6. Miró P, Audiffred M, Heine T. An atlas of two-dimensional materials. *Chem Soc Rev* 2014, 43:6537–6554.

7. Butler SZ, Hollen SM, Cao L, Cui Y, Gupta JA, Gutiérrez HR, Heinz TF, Hong SS, Huang J, Ismach AF, et al. Progress, challenges, and opportunities in

two-dimensional materials beyond graphene. *ACS Nano* 2013, 7:2898–2926.

8. Gupta A, Sakthivel T, Seal S. Recent development in 2D materials beyond graphene. *Prog Mater Sci* 2015, 73:44–126.

9. Chen W, Li Y, Yu G, Zhou Z, Chen Z. Electronic structure and reactivity of boron nitride nanoribbons with Stone-Wales defects. *J Chem Theory Comput* 2009, 5:3088–3095.

10. Tang Q, Zhou Z, Chen Z. Molecular charge transfer: a simple and effective route to engineer the band structures of BN nanosheets and nanoribbons. *J Phys Chem C* 2011, 115:18531–18537.

11. Chen W, Li Y, Yu G, Li C, Zhang SB, Zhou Z, Chen Z. Hydrogenation: a simple approach to realize semiconductor-half-metal-metal transition in boron nitride nanoribbons. *J Am Chem Soc* 2010, 132:1699–1705.

12. Freeman C, Claeyssens F, Allan N, Harding J. Graphitic nanofilms as precursors to wurtzite films: theory. *Phys Rev Lett* 2006, 96:066102.

13. Wu X, Pei Y, Zeng XC. B_2C graphene, nanotubes, and nanoribbons. *Nano Lett* 2009, 9:1577–1582.

14. Li Y, Li F, Zhou Z, Chen Z. SiC_2 silagraphene and its one-dimensional derivatives: where planar tetracoordinate silicon happens. *J Am Chem Soc* 2011, 133:900–908.

15. Tusche C, Meyerheim H, Kirschner J. Observation of depolarized ZnO(0001) monolayers: formation of unreconstructed planar sheets. *Phys Rev Lett* 2007, 99:026102.

16. Wang Z, Li H, Liu Z, Shi Z, Lu J, Suenaga K, Joung SK, Okazaki T, Gu Z, Zhou J, et al. Mixed low-dimensional nanomaterial: 2D ultranarrow MoS_2 inorganic nanoribbons encapsulated in quasi-1D carbon nanotubes. *J Am Chem Soc* 2010, 132:13840–13847.

17. Kresse G, Furthmullerr J. Efficient iterative schemes for *ab initio* total-energy calculations using a plane-wave basis set. *Phys Rev B* 1996, 54:11169–11186.

18. Delley B. From molecules to solids with the DMol (3) approach. *J Chem Phys* 2000, 113:7756–7764.

19. Perdew JP, Burke K, Ernzerhof M. Generalized gradient approximation made simple. *Phys Rev Lett* 1996, 77:3865–3868.

20. Ceperley DM, Alder BJ. Ground-state of the electron-gas by a stochastic method. *Phys Rev Lett* 1980, 45:566–569.

21. Heyd J, Scuseria GE, Ernzerhof M. Hybrid functionals based on a screened Coulomb potential. *J Chem Phys* 2003, 118:8207.

22. Jain M, Chelikowsky JR, Louie SG. Reliability of hybrid functionals in predicting band gaps. *Phys Rev Lett* 2011, 107:216806.

23. Grimme S. Semiempirical GGA-type density functional constructed with a long-rang dispersion correction. *J Comput Chem* 2007, 27:1787–1799.

24. Gräfenstein J, Cremer D. An efficient algorithm for the density-functional theory treatment of dispersion interactions. *J Chem Phys* 2009, 130:124105.

25. Grimme S, Antony J, Ehrlich S, Krieg H. A consistent and accurate ab initio parametrization of density functional dispersion correction (DFT-D) for the 94 elements H-Pu. *J Chem Phys* 2010, 132:154104.

26. Cococcioni M, de Gironcoli S. Linear response approach to the calculation of the effective interaction parameters in the LDA + U method. *Phys Rev B* 2005, 71:035105.

27. Coleman JN, Lotya M, O'Neill A, Bergin SD, King PJ, Khan U, Young K, Gaucher A, De S, Smith RJ, et al. Two-dimensional nanosheets produced by liquid exfoliation of layered materials. *Science* 2011, 331:568–571.

28. Balendhran S, Deng J, Ou JZ, Walia S, Scott J, Tang J, Wang KL, Field MR, Russo S, Zhuiykov S, et al. Enhanced charge carrier mobility in two-dimensional high dielectric molybdenum oxide. *Adv Mater* 2013, 25:109–114.

29. Watanabe K, Taniguchi T, Kanda H. Direct-bandgap properties and evidence for ultraviolet lasing of hexagonal boron nitride single crystal. *Nat Mater* 2004, 3:404–409.

30. Watanabe K, Taniguchi T, Niiyama T, Miya K, Taniguchi M. Far-ultraviolet plane-emission handheld device based on hexagonal boron nitride. *Nat Photonics* 2009, 3:591–594.

31. Zhu Y, Bando Y, Yin L, Golberg D. Field nanoemitters: ultrathin BN nanosheets protruding from Si_3N_4 nanowires. *Nano Lett* 2006, 6:2982–2986.

32. Zhi C, Bando Y, Tang C, Kuwahara H, Golberg D. Large-scale fabrication of boron nitride nanosheets and their utilization in polymeric composites with improved thermal and mechanical properties. *Adv Mater* 2009, 21:2889–2893.

33. Dean CR, Young AF, Meric I, Lee C, Wang L, Sorgenfrei S, Watanabe K, Taniguchi T, Kim P, Shepard KL, et al. Boron nitride substrates for high-quality graphene electronics. *Nat Nanotech* 2010, 5:722–726.

34. Britnell L, Gorbachev RV, Jalil R, Belle BD, Schedin F, Katsnelson MI, Eaves L, Morozov SV, Mayorov AS, Peres NMR, et al. Electron tunneling through ultrathin boron nitride crystalline barriers. *Nano Lett* 2012, 12:1707–1710.

35. Zeng H, Zhi C, Zhang Z, Wei X, Wang X, Guo W, Bando Y, Golberg D. 'White graphenes': boron nitride nanoribbons via boron nitride nanotube unwrapping. *Nano Lett* 2010, 10:5049–5055.

36. Erickson KJ, Gibb AL, Sinitskii A, Rousseas M, Alem N, Tour JM, Zettl AK. Longitudinal splitting of boron nitride nanotubes for the facile synthesis of high quality boron nitride nanoribbons. *Nano Lett* 2011, 11:3221–3226.

37. Li L, Li LH, Chen Y, Dai XJ, Lamb PR, Cheng BM, Lin MY, Liu X. High-quality boron nitride nanoribbons: unzipping during nanotube synthesis. *Angew Chem Int Ed* 2013, 52:4212–4216.

38. Barone V, Peralta JE. Magnetic boron nitride nanoribbons with tunable electronic properties. *Nano Lett* 2008, 8:2210–2214.

39. Kan E, Wu F, Xiang H, Yang J, Whangbo MH. Half-metallic dirac point in B-edge hydrogenated BN nanoribbons. *J Phys Chem C* 2011, 115:17252–17254.

40. Lai L, Lu J, Wang L, Luo G, Zhou J, Qin R, Gao Z, Mei WN. Magnetic properties of fully bare and half-bare boron nitride nanoribbons. *J Phys Chem C* 2009, 113:2273–2276.

41. Jin C, Lin F, Suenaga K, Iijima S. Fabrication of a free-standing boron nitride single layer and its defect assignments. *Phys Rev Lett* 2009, 102:195505.

42. Zhang HX, Feng PX. Controlling bandgap of rippled hexagonal boron nitride membranes via plasma treatment. *ACS Appl Mater Interfaces* 2012, 4:30–33.

43. Tang Q, Zhou Z, Shen P, Chen Z. Band gap engineering of BN sheets by interlayer dihydrogen bonding and electric field control. *Chem Phys Chem* 2013, 14:1787–1792.

44. Tang Q, Bao J, Li Y, Zhou Z, Chen Z. Tuning band gaps of BN nanosheets and nanoribbons via interfacial dihalogen bonding and external electric field. *Nanoscale* 2014, 6:8624–8634.

45. Splendiani A, Sun L, Zhang Y, Li T, Kim J, Chim C, Galli G, Wang F. Emerging photoluminescence in monolayer MoS_2. *Nano Lett* 2010, 10:1271–1275.

46. Radisavljevic B, Radenovic A, Brivio J, Giacometti V, Kis A. Single-layer MoS_2 transistors. *Nat Nanotech* 2011, 6:147–150.

47. Yin Z, Li H, Li H, Jiang L, Shi Y, Sun Y, Lu G, Zhang Q, Chen X, Zhang H. Single-layer MoS_2 phototransistors. *ACS Nano* 2012, 6:74–80.

48. Radisavljevic B, Whitwick MB, Kis A. Integrated circuits and logic operations based on single-layer MoS_2. *ACS Nano* 2011, 5:9934–9938.

49. Li Y, Zhou Z, Zhang S, Chen Z. MoS_2 nanoribbons: high stability and unusual electronic and magnetic properties. *J Am Chem Soc* 2008, 130:16739–16744.

50. Erdogan E, Popov IH, Enyashin AN, Seifert G. Transport properties of MoS_2 nanoribbons: edge priority. *Eur Phys J B* 2012, 85:33.

51. Liu Q, Li L, Li Y, Gao Z, Chen Z, Lu J. Tuning electronic structure of bilayer MoS_2 by vertical electric field: a first-principles investigation. *J Phys Chem C* 2012, 116:21556–21562.

52. Johari P, Shenoy VB. Tuning the electronic properties of semi-conducting transition metal dichalcogenides by applying mechanical strains. *ACS Nano* 2012, 6:5449–5456.

53. Ataca C, Ciraci S. Functionalization of single-layer MoS_2 honeycomb structures. *J Phys Chem C* 2011, 115:13303–13311.

54. Komsa HP, Kotakoski J, Kurasch S, Lehtinen O, Kaiser U, Krasheninnikov AV. Two-dimensional transition metal dichalcogenides under electron irradiation: defect production and doping. *Phys Rev Lett* 2012, 109:035503.

55. He Q, Zeng Z, Yin Z, Li H, Wu S, Huang X, Zhang H. Fabrication of flexible MoS_2 thin-film transistor arrays for practical gas-sensing applications. *Small* 2012, 8:2994–2999.

56. Li Y, Wu D, Zhou Z, Cabrera CR, Chen Z. Enhanced Li adsorption and diffusion on MoS_2 zigzag nanoribbons by edge effects: a computational study. *J Phys Chem Lett* 2012, 3:2221–2227.

57. Jing Y, Zhou Z, Cabrera CR, Chen Z. Metallic VS_2 monolayer: a promising 2D anode material for lithium ion batteries. *J Phys Chem C* 2013, 117:25409–25413.

58. Li F, Cabrera CR, Chen Z. Theoretical design of MoO_3-based high-rate lithium ion battery electrodes: the effect of dimensionality reduction. *J Mater Chem A* 2014, 2:19180–19188.

59. Chernova NA, Roppolo M, Dillon AC, Whittingham MS. Layered vanadium and molybdenum oxides: batteries and electrochromics. *J Mater Chem* 2009, 19:2526–2552.

60. Sreedhara MB, Matte HSSR, Govindaraj A, Rao CNR. Synthesis, characterization, and properties of few-layer MoO_3. *Chem Asian J* 2013, 8:2430–2435.

61. Balendhran S, Walia S, Alsaif M, Nguyen EP, Ou JZ, Zhuiykov S, Sriram S, Bhaskaran M, Kalantar-zadeh K. Field effect biosensing platform based on 2D α-MoO_3. *ACS Nano* 2013, 7:9753–9760.

62. Sha X, Chen L, Cooper AC, Pez GP, Cheng H. Hydrogen absorption and diffusion in bulk α-MoO_3. *J Phys Chem C* 2009, 113:11399–11407.

63. Li F, Chen Z. Tuning electronic and magnetic properties of MoO_3 sheets by cutting, hydrogenation, and external strain: a computational investigation. *Nanoscale* 2013, 5:5321–5333.

64. Hu XK, Qian YT, Song ZT, Huang JR, Cao R, Xiao JQ. Comparative study on MoO_3 and H_xMoO_3 nanobelts: structure and electric transport. *Chem Mater* 2008, 20:1527–1533.

65. Tang Q, Li F, Zhou Z, Chen Z. Versatile electronic and magnetic properties of corrugated V_2O_5 two-dimensional crystal and its derived one-dimensional nanoribbons: a computational exploration. *J Phys Chem C* 2011, 115:11983–11990.

66. Negreira AS, Aboud S, Wilcox J. Surface reactivity of $V_2O_5(001)$: effects of vacancies, protonation, hydroxylation, and chlorination. *Phys Rev B* 2011, 83:045423.

67. Rui X, Lu Z, Yu H, Yang D, Hng HH, Lim TM, Yan Q. Ultrathin V_2O_5 nanosheet cathodes: realizing ultrafast reversible lithium storage. *Nanoscale* 2013, 5:556–560.

68. Wang Z, Su Q, Deng H. Single-layered V_2O_5 a promising cathode material for rechargeable Li and Mg ion batteries: an ab initio study. *Phys Chem Chem Phys* 2013, 15:8705–8709.

69. Du AJ, Smith SC, Yao XD, Sun CH, Li L, Lu GQ. The role of V_2O_5 on the dehydrogenation and hydrogenation in magnesium hydride: an ab initio study. *Appl Phys Lett* 2008, 92:163106.

70. Tang Q, Li Y, Zhou Z, Chen Y, Chen Z. Tuning electronic and magnetic properties of wurtzite ZnO nanosheets by surface hydrogenation. *ACS Appl Mater Interfaces* 2010, 2:2442–2447.

71. Chen Q, Wang J, Zhu L, Wang S, Ding F. Fluorination induced half metallicity in two-dimensional few zinc oxide layers. *J Chem Phys* 2010, 132:204703.

72. Tang Q, Cui Y, Li Y, Zhou Z, Chen Z. How do surface and edge effects alter the electronic properties of GaN nanoribbons? *J Phys Chem C* 2011, 115:1724–1731.

73. Wu W, Lu P, Zhang Z, Guo W. Electronic and magnetic properties and structural stability of BeO sheet and nanoribbons. *ACS Appl Mater Interfaces* 2011, 3:4787–4795.

74. Naguib M, Kurtoglu M, Presser V, Lu J, Niu J, Heon M, Hultman L, Gogotsi Y, Barsoum MW. Two-dimensional nanocrystals produced by exfoliation of Ti_3AlC_2. *Adv Mater* 2011, 23:4248–4253.

75. Naguib M, Mashtalir O, Carle J, Presser V, Lu J, Hultman L, Gogotsi Y, Barsoum MW. Two-dimensional transition metal carbides. *ACS Nano* 2012, 6:1322–1331.

76. Naguib M, Halim J, Lu J, Cook KM, Hultman L, Gogotsi Y, Barsoum MW. New two-dimensional niobium and vanadium carbides as promising materials for Li-ion batteries. *J Am Chem Soc* 2013, 135:15966–15969.

77. Tang Q, Zhou Z, Shen P. Are MXenes promising anode materials for Li ion batteries? Computational studies on electronic properties and Li storage capability of Ti_3C_2 and $Ti_3C_2X_2$ (X = F, OH) monolayer. *J Am Chem Soc* 2012, 134:16909–16916.

78. Naguib M, Mochalin VN, Barsoum MW, Gogotsi Y. MXenes: a new family of two-dimensional materials. *Adv Mater* 2014, 26:992–1005.

79. Khazaei M, Arai M, Sasaki T, Chung C, Venkataramanan NS, Estili M, Sakka Y, Kawazoe Y. Novel electronic and magnetic properties of two-dimensional transition metal carbides and nitrides. *Adv Funct Mater* 2013, 23:2185–2192.

80. Xie Y, Naguib M, Mochalin VN, Barsoum MW, Gogotsi Y, Yu X, Nam KW, Yang XQ, Kolesnikov AI, Kent PRC. Role of surface structure on Li-ion energy storage capacity of two-dimensional transition-metal carbides. *J Am Chem Soc* 2014, 136:6385–6394.

81. Mashtalir O, Naguib M, Mochalin VN, Dall'agnese Y, Heon M, Barsoum MW, Gogotsi Y. Intercalation and delamination of layered carbides and carbonitrides. *Nat Commun* 2013, 4:1716.

82. Lukatskaya MR, Mashtalir O, Ren CE, Dall'Agnese Y, Rozier P, Taberna PL, Naguib M, Simon P, Barsoum MW, Gogotsi Y. Cation intercalation and high volumetric capacitance of two-dimensional titanium carbide. *Science* 2013, 341:1502–1505.

83. Ghidiu M, Lukatskaya MR, Zhao MQ, Gogotsi Y, Barsoum MW. Conductive two-dimensional titanium carbide 'clay' with high volumetric capacitance. *Nature* 2014, 516:78–81.

84. Xie X, Chen S, Ding W, Nie Y, Wei Z. An extraordinarily stable catalyst: Pt NPs supported on two-dimensional $Ti_3C_2X_2$ (X = OH, F) nanosheets for oxygen reduction reaction. *Chem Commun* 2013, 49:10112–10114.

85. Hu Q, Sun D, Wu Q, Wang H, Wang L, Liu B, Zhou A, He J. MXene: a new family of promising hydrogen storage medium. *J Phys Chem A* 2013, 117:14253–14260.

86. Halim J, Lukatskaya MR, Cook KM, Lu J, Smith CR, Näslund LÅ, May SJ, Hultman L, Gogotsi Y, Eklund P, et al. Transparent conductive two-dimensional titanium carbide epitaxial thin films. *Chem Mater* 2014, 26:2374–2381.

87. Peng Q, Guo J, Zhang Q, Xiang J, Liu B, Zhou A, Liu R, Tian Y. Unique lead adsorption behavior of activated hydroxyl group in two-dimensional titanium carbide. *J Am Chem Soc* 2014, 136:4113–4116.

88. Er D, Li J, Naguib M, Gogotsi Y, Shenoy VB. Ti_3C_2 MXene as a high capacity electrode material for metal (Li, Na, K, Ca) ion batteries. *ACS Appl Mater Interfaces* 2014, 6:11173–11179.

89. Ma ZN, Hu ZP, Zhao XD, Tang Q, Wu DH, Zhou Z, Zhang LX. Tunable band structures of heterostructured bilayers with transition metal dichalcogenide and MXene monolayer. *J Phys Chem C* 2014, 118:5593–5599.

90. Xie Y, Dall'Agnese Y, Naguib M, Gogotsi Y, Barsoum MW, Zhuang HL, Kent PRC. Prediction and characterization of MXene nanosheet anodes for non-lithium-ion batteries. *ACS Nano* 2014, 8:9606–9615.

91. Wang X, Shen X, Gao Y, Wang Z, Yu R, Chen L. Atomic-scale recognition of surface structure and intercalation mechanism of Ti_3C_2X. *J Am Chem Soc* 2015, 137:2715–2721.

92. Hoffmann R, Alder RW, Wilcox CF. Planar tetracoordinate carbon. *J Am Chem Soc* 1970, 92:4992–4993.

93. Dai J, Li Z, Yang J, Hou J. A first-principles prediction of two-dimensional superconductivity in pristine B_2C single layers. *Nanoscale* 2012, 4:3032–3035.

94. An H, Liu C, Zeng Z, Fan C, Ju X. Li-doped B_2C graphene as potential hydrogen storage medium. *Appl Phys Lett* 2011, 98:173101.

95. Guo YH, Xu B, Xia YD, Yin J, Liu ZG. First-principles study of hydrogen storage on Ti-decorated B_2C sheet. *J Solid State Chem* 2012, 190:126–129.

96. Tan X, Li F, Chen Z. Metallic BSi_3 silicene and its one-dimensional derivatives: unusual nanomaterials with planar aromatic D6h six-membered silicon rings. *J Phys Chem C* 2014, 118:25825–25835.

97. Tan X, Cabrera CR, Chen Z. Metallic BSi_3 silicene: a promising high capacity anode material for lithium-ion batteries. *J Phys Chem C* 2014, 118:25836–25843.

98. Zhang S, Yan Z, Li Y, Chen Z, Zeng H. Atomically thin arsenene and antimonene: semimetal–semiconductor and indirect–direct band-gap transitions. *Angew Chem Int Ed* 2015, 54:3112–3115.

99. Amo-Ochoa P, Welte L, Gonzalez-Prieto R, Sanz Miguel PJ, Gomez-Garcia CJ, Mateo-Marti E, Delgado S, Gomez-Herrero J, Zamora F. Single layers of a multifunctional laminar Cu(I,II) coordination polymer. *Chem Commun* 2010, 46:3262–3264.

100. Abel M, Clair S, Ourdjini O, Mossoyan M, Porte L. Single layer of polymeric Fe-phthalocyanine: an organometallic sheet on metal and thin insulating film. *J Am Chem Soc* 2011, 133:1203–1205.

101. Kambe T, Sakamoto R, Hoshiko K, Takada K, Miyachi M, Ryu JH, Sasaki S, Kim J, Nakazato K, Takata M, et al. π-Conjugated nickel bis(dithiolene) complex nanosheet. *J Am Chem Soc* 2013, 135:2462–2465.

102. Tang Q, Zhou Z, Chen Z. Single-layer $[Cu_2Br(IN)_2]_n$ coordination polymer (CP): electronic and magnetic properties, and implication for molecular sensors. *J Phys Chem C* 2012, 116:4119–4125.

103. Zhou J, Sun Q. Magnetism of phthalocyanine-based organometallic single porous sheet. *J Am Chem Soc* 2011, 133:15113–15119.

104. Lv K, Zhou J, Zhou L, Chen XS, Chan SH, Sun Q. Pre-combustion CO_2 capture by transition metal ions embedded in phthalocyanine sheets. *J Chem Phys* 2012, 136:234703.

105. Deng Q, Zhao L, Gao X, Zhang M, Luo Y, Zhao Y. Single layer of polymeric cobalt phthalocyanine: promising low-cost and high-activity nanocatalysts for CO oxidation. *Small* 2013, 9:3506–3513.

106. Tang Q, Zhou Z. Electronic properties of π-conjugated nickel bis(dithiolene) network and its addition reactivity with ethylene. *J Phys Chem C* 2013, 117:14125–14129.

107. Wang ZF, Su N, Liu F. Prediction of a two-dimensional organic topological insulator. *Nano Lett* 2013, 13:2842–2845.

108. Zhou Q, Wang J, Chwee TS, Wu G, Wang X, Ye Q, Xu J, Yang SW. Topological insulators based on 2D shape-persistent organic ligand complexes. *Nanoscale* 2015, 7:727–735.